Sensors and Materials, Vol. 36, No. 3 (2024) 1047–1064
MYU Tokyo

S & M 3580

Development of Wind Wake-effect Minimizing Model Based on Combination of Dung Beetle Optimization, Extreme Learning Machine, and Genetic Algorithms

Li-Nan Qu,[1,2] Hao-Peng Li,[3] Hsiung-Cheng Lin,[4*] and Ling-Ling Li[1]

[1]State Key Laboratory of Reliability and Intelligence of Electrical Equipment, Hebei University of Technology, Tianjin 300401, China
[2]China Electrical Equipment Research Institute of Science and Technology Co., Ltd., Shanghai 200436, China
[3]School of Electronic and Information Engineering, Hebei University of Technology, Tianjin 300401, China
[4]Department of Electronic Engineering, National Chin-Yi University of Technology, Taichung 41170, Taiwan

(Received October 7, 2023; accepted February 16, 2024)

Keywords: wind speed and direction sensor, wind farm optimization layout, Monte Carlo simulation, genetic algorithm, dung beetle optimization algorithm

The wake effect caused by a wind turbine can reduce the wind speed and add turbulence to the wind, thus impacting the power generation efficiency. To effectively enhance the generated power in wind farms, we propose an optimal layout model that is combined with artificial intelligence optimizing algorithms. First, the adaptive genetic algorithm (AGA) is used to optimize the collected wind speed and direction distribution data as the optimization basis. Second, the extreme learning machine (ELM) based on Monte Carlo simulation is used to establish a guidance for determining the turbine relocation from the optimization basis. Simultaneously, the dung beetle optimization (DBO) algorithm is developed to improve the performance of ELM for achieving the optimal solution. The proposed model was tested at six different wind farms and under three different wind condition distribution settings. The simulation results verify that the model is superior to existing algorithms in reducing the wake-effect impact as well as optimizing the wind farm layout.

1. Introduction

In recent years, under the dual pressure of an energy crisis and environmental protection, renewable energy has developed rapidly in many countries. As a clean, pollution-free, and low-cost energy with unlimited reserves that can be employed worldwide, wind energy and its related problems have attracted widespread interest. To make full use of the land, wind farms usually operate multiple turbines. However, owing to the wake effect, it is difficult to operate many turbines in the wind farm at the optimal power generation point, resulting in a certain degree of waste. How to avoid or minimize the impact of the wake effect is a research hotspot in the field of wind power.

*Corresponding author: e-mail: hclin@ncut.edu.tw
https://doi.org/10.18494/SAM4701

ISSN 0914-4935

At present, there are two main technologies to alleviate the negative impact of the wake effect.[1] One method is wind farm control, that is, when the wind farm is established, the control of the wake is achieved by adjusting the operation strategy of the turbine.

The second method is the optimization of the wind farm layout, that is, after selecting the location of wind farm construction, the location of turbine deployment is determined by considering various factors such as terrain, wind condition distribution, and turbine rotor plane so as to reduce the influence of the wake.[2] In recent years, with the increasing number of turbines to be built in wind farms, the problem of wind farm layout optimization has become more and more complex, and the problem has been proved to be a nondeterministic polynomial and nonconvex problem.[3] Therefore, linear and mixed integer programming methods may not be able to yield the optimal optimization results.[4,5]

With the development of wind speed and direction sensor technology and computational intelligence technology, the calculation of long-term wind distribution data is becoming more and more accurate. At the same time, because the analytical model of the wake involves a large number of constraints, many studies have widely applied intelligent optimization methods to solve the problem of the optimal layout of a wind farm.[6] For example, Kusiak and Song[7] defined the turbine layout design as a two-objective problem and proposed a multi-objective evolutionary strategy algorithm to solve it. On the basis of the work of Kusiak and Song,[7] Eroglu and Seckiner[8] used an ant colony algorithm to obtain a layout that can make the total output power larger. The particle swarm optimization algorithm also shows good advantages in solving the problem of wind farm layout optimization. Many groups have made numerous attempts and have achieved good results.[9–11]

The genetic algorithm (GA) is an algorithm derived from natural evolution theory. It selects the most suitable individuals (solutions) for reproduction and iteration through mutation, crossover, and other operations. GA has become the most popular algorithm in wind farm layout optimization.[12] As early as 1994, Mosetti *et al.*[13] proposed a GA-based method to optimize the layout of wind farms, which was the beginning of offshore wind farm optimization. In recent years, many groups have used GA to solve various wind farm layout optimization problems, and achieved good results.[14–16] A combination method based on GA has been applied to wind farm layout optimization.[17,18]

Although the conventional GA (CGA) has shown good performance for the wind farm layout problem, some studies have revealed that the algorithm still has much room for improvement. Ju *et al.*[17] believed that CGA should be modified to solve the problem of optimal layout of wind farms. Liu and Wang[19] proposed an adaptive GA (AGA) to relocate the worst turbine. The positioning method was random positioning, which shows good performance for the layout. On the basis of their research, in this study, we further explore the positioning method of the worst turbine and use the power response surface of the extreme learning machine (ELM) approximation to provide guidance. Note that in many studies on the layout optimization of wind farms, the selected wind farm area is assumed to be an extended continuous area. However, there are 'unavailable' areas in most actual wind farms, such as areas of unsafe erection terrain. If the wind farm has a small land area that does not belong to the common unit, the wind farm developer needs to negotiate the compensation amount with these small land owners (the amount

of compensation must take into account many factors, and the goal is to maximize the benefits of wind farms). When there are differences between wind farm developers and these small land owners in negotiating the amount of compensation, there will be undevelopable areas. We call the above 'unavailable' areas 'restricted' areas. In a wind farm with a 'forbidden zone', wind farm planners need to fully analyze and consider the value of each smaller unit of the wind farm. Therefore, there is an urgent need for a wind farm layout algorithm that is fast and can fully explore the existence of forbidden zones. With the gradual maturation of offshore wind turbine technology, the development of turbine repositioning technology will also become more valuable.[20]

The contributions of this study are as follows. Firstly, the wind condition distribution data signal obtained by the wind speed and direction sensor is used to determine the individual's ability to adapt to the environment in nature, which is used for reference, and the power distribution response surface is obtained by using ELM to predict the power as guidance information. An improved GA ELM-GA specifically applied to wind farm layout optimization is proposed. Secondly, because of the randomness of the ELM parameters, the prediction results are suboptimal. We use the dung beetle optimization (DBO) algorithm to optimize the parameters. Finally, we consider the problem of possible forbidden zones in wind farms, and use the proposed algorithm on six types of wind farm with forbidden zones as a test. The results show that the proposed method can minimize the wake effect while avoiding the deployment of turbines to the forbidden zone, which has a great positive impact on the initial investment.

The rest of this study is organized as follows. In Sect. 2, we introduce the concepts of the DBO algorithm and ELM algorithm, and then briefly review the wake modeling method. In Sect. 3, the wind farm optimization layout problem is formulated, and the GA combined with DBO ELM (DBO-ELM-GA) is developed. The experimental results are analyzed and discussed in Sect. 4. In Sect. 5, we summarize the contribution of this article.

2. Methodology

2.1 Description of fundamental modeling

To balance the calculation cost and calculation accuracy, we apply the PARK model to simulate the aerodynamics of the wind farm.[21] Here, the DBO algorithm is used to optimize the parameters of ELM. It has five different update rules based on the ball rolling, dancing, foraging, stealing, and breeding behavior of dung beetles. Since the algorithm is not the focus of this article, we do not give a detailed introduction. Interested readers may refer to Ref. 22.

Different from conventional feedforward neural networks, ELM randomly selects input weights and hidden layer biases, and calculates output weights on the basis of the generalized inverse matrix theory.[23] It has the characteristics of fast learning speed and small training error. We use the quasi-Newton method to optimize the weight matrix of ELM. The definition of equivariant regularization (ER) loss is expressed as follows:

$$L_{ER} = \frac{1}{n}\sum_{i=1}^{n} \begin{cases} \tau\left(y_{(t)} - \hat{y}_{(t)}\right)^2, & y_{(t)} > \hat{y}_{(t)} \\ (1-\tau)\left(y_{(t)} - \hat{y}_{(t)}\right)^2, & \text{otherwise} \end{cases} \tag{1}$$

where n is the number of samples; τ is a weight parameter used to adjust the loss; $\hat{y}_{(t)}$ is the predicted value of the t sample; and $y_{(t)}$ is the true value of the t sample.

2.2 Modeling of wind farm layout optimization problem

2.2.1 Objective function of optimizing the wind farm layout problem

The goal of optimizing the wind farm layout is to select the location of the wind turbine installation site before the wind farm construction is established, taking into account the terrain conditions, such as areas where layout is not possible or prohibited, to maximize the overall wind farm power output.

Mosetti *et al.*[13] defines the objective function of this problem as

$$\begin{aligned} \min_{N,\phi} \frac{\varsigma_{tot}(N)}{\vartheta_{tot}(N,\phi)} \text{ s.t. } \varsigma_{tot}(N) &= N\left(\frac{2}{3} + \frac{1}{3}e^{-0.00174N^2}\right)\vartheta_{tot}(N,\phi) \\ &= \sum_{i=1}^{N}\sum_{\theta,v} p(\theta,v)\vartheta_i(\theta,v,\phi), \end{aligned} \tag{2}$$

where the number of turbines expected to be set is N, and ϕ represents a feasible turbine location layout. $\vartheta_{tot}(N, \phi)$ is set as the total power generation of the wind farm with N turbines in the case of layout ϕ. v and θ are the wind speed and wind direction data obtained by the wind speed and wind direction sensor, respectively. $p(\theta, v)$ is the probability distribution that wind speed v and wind direction θ occur simultaneously. $\vartheta_i(\theta, v, \phi)$ is the power generation of the i turbine when the wind farm layout is ϕ and the wind direction and wind speed are θ and v, respectively. $\varsigma_{tot}(N)$ is the total cost of N turbines.

The objective function is also equivalent to maximizing the power generation of the wind farm. The variable to be optimized is layout ϕ, and the formula is as follows.

$$\max_{\phi} \vartheta_{tot}(\phi) \text{ s.t. } \vartheta_{tot}(\phi) = \sum_{i=1}^{N}\sum_{\theta,v} p(\theta,v)\vartheta_i(\theta,v,\phi) \tag{3}$$

2.2.2 Constraints in wind farm layout problem

Usually, the land for the construction of wind farms has small areas unsuitable to install turbines, i.e., forbidden zones. As shown in Fig. 1, among 144 square cells, the white cells represent suitable areas where turbines can be placed, and shaded cells (cell indexes 31, 37, 59, 60, 72, 102, 113, 114, 133) are forbidden zones.

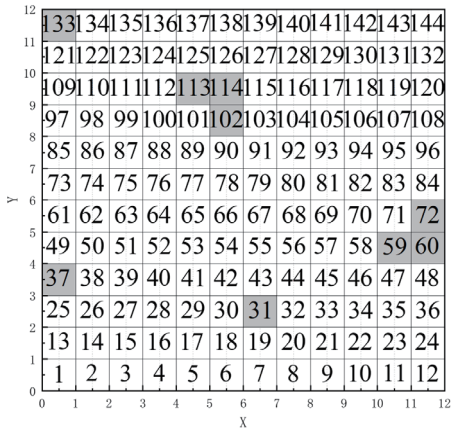

Fig. 1. Schematic diagram of wind farm with forbidden zones (without turbine).

2.2.3 Wind farm modeling

As shown in Fig. 1, the wind farm layout cells are mapped into a two-dimensional coordinate system.

Firstly, the row and column index coordinate system based on wind farm cells is defined. X_i and Y_i are defined as the row and column indices in the coordinate system, respectively. For each $i \in I$, the corresponding coordinate in the coordinate system is (X_i, Y_i), and the calculation formula is expressed as

$$X_i = i - S_r \cdot \left\lfloor \frac{i-1}{S_r} \right\rfloor - 1, \tag{4}$$

$$Y_i = \left\lfloor \frac{i-1}{S_r} \right\rfloor, \tag{5}$$

where S_r is the number of row cells in the coordinate system and is set to 12 in this study, and $\lfloor \varpi \rfloor$ represents the maximum integer not greater than ϖ.

All cells can be represented as the following matrix:

$$S_I = \begin{bmatrix} X_1 & X_2 & \cdots & X_{S\kappa} \\ Y_1 & Y_2 & \cdots & Y_{S\kappa} \end{bmatrix}, \tag{6}$$

where $S\kappa = 144$ represents the number of suitable cells for turbines in the wind farm.

The second coordinate system is a coordinate system indexed by the actual position of the turbine in the wind farm. Similar to the first coordinate system, the coordinate of turbine i is (x_i, y_i), and the formula is expressed as

$$x_i = \left(i - S_r \cdot \left\lfloor \frac{i-1}{S_r} \right\rfloor - 0.5 \right) \cdot W_c, \tag{7}$$

$$y_i = \left(\left\lfloor \frac{i-1}{S_r} \right\rfloor + 0.5 \right) \cdot W_c, \tag{8}$$

where W_c is the width of the cell. All the actual position coordinates can be expressed as the following matrix.

$$S_A = \begin{bmatrix} x_1 & x_2 & \cdots & x_{S\kappa} \\ y_1 & y_2 & \cdots & y_{S\kappa} \end{bmatrix} \tag{9}$$

The third coordinate system is composed of the second coordinate system rotated clockwise by θ as a whole. Similar to the first two coordinate systems, in this coordinate system, the coordinate of turbine i is (x_i^θ, y_i^θ), which can be calculated using (x_i, y_i), and the expression is

$$\begin{bmatrix} x_i^\theta \\ y_i^\theta \end{bmatrix} = \begin{bmatrix} \cos\theta & -\sin\theta \\ \sin\theta & \cos\theta \end{bmatrix} \begin{bmatrix} x_i \\ y_i \end{bmatrix}. \tag{10}$$

All actual position coordinates are represented as the following matrix.

$$S_A^\theta = \begin{bmatrix} x_1^\theta & x_2^\theta & \cdots & x_{S\kappa}^\theta \\ y_1^\theta & y_2^\theta & \cdots & y_{S\kappa}^\theta \end{bmatrix} \tag{11}$$

2.3 ELM-based guidance model

On the basis of Monte Carlo simulation,[24] ELM is used to establish a guidance model in this study. Firstly, Monte Carlo simulation generates 10000 random layouts and calculates the power output of the turbine when the turbine is placed at coordinate (X_i, Y_i). Secondly, the average power output of each cell is calculated. ELM is used to construct the response surface to approximate the expected power probability distribution on the basis of the location of each turbine. Finally, a Monte Carlo-based ELM guided response surface is formed for a specific wind farm area to be constructed.

2.4 Optimization of wind farm layout algorithm

DBO-ELM-GA based on CGA and AGA[19] is introduced in this study.

2.4.1 CGA

The steps of using CGA to optimize the layout of wind farms are as follows, in which the ranges of elite rate R_e, selection rate R_s, and mutation rate R_m are set to (0, 1].

Step 1: Initialize a population $\left\{\phi_j^k\right\}_{j=1}^{N_p}$ with the total number N_p, where k is the number of iterations, and the initial value is 0.

Step 2: Calculate the fitness value of all individuals ϕ_j^k in the population, and sort the individuals in the order of fitness from large to small.

Step 3: Firstly, retain some of the best individuals as the parent class. The retention ratio is determined in accordance with the elite rate R_e, that is, $R_e \cdot N_p$ best individuals are retained for the next-generation population, and then $R_s \cdot N_p$ individuals are randomly selected from other individuals to fill the remaining parent class positions.

Step 4: In accordance with the crossover rate R_c, two individuals in the parent class are randomly selected for crossover operation to generate new individuals for the next generation until the population size reaches N_p.

Step 5: Randomly select individuals on the basis of the mutation rate R_m, and then randomly select the position i of the turbine among these individuals, and move these turbines at position i to a turbine-less position j.

Step 6: Determine whether the GA converges. If it converges, terminate the GA; otherwise, return to Step 2.

2.4.2 AGA

AGA adds a step called worst turbine relocation between steps 3 and 4 of CGA. The turbine with the lowest power output is moved to other random positions.

2.4.3 DBO-ELM-GA

Although the random repositioning method of AGA can ensure exploration efficiency, it is usually difficult to converge to an optimal layout. Therefore, similar to AGA, DBO-ELM-GA adds the worst turbine repositioning step guided by DBO-ELM between steps 3 and 4 of CGA. This step moves the turbine with the lowest power output by two strategies: the same random selection strategy as AGA and the guided selection strategy based on the DBO-ELM power prediction model. In a certain iteration process, the selection of these two strategies is determined on the basis of a predetermined threshold δ ($0 \le \delta \le 1$). Before the beginning of each iteration, a random number δ^* ($0 \le \delta^* \le 1$) is generated, and then whether or not the number is greater than δ is judged. If it is greater than δ, the guiding selection strategy based on the DBO-ELM power prediction model is performed; otherwise, the random selection strategy is performed.

If the value of δ is too large ($\delta \approx 1$), the algorithm relies entirely on the DBO-ELM power prediction model to select a new position. Although it will accelerate convergence, it may cause the agent to fall into a local optimum. If δ is set too small ($\delta \approx 1$), the algorithm is basically equivalent to AGA. Therefore, the A value should be set reasonably to achieve a good balance between exploration and development.

For the guidance selection strategy based on the DBO-ELM power prediction model, firstly, N_{can} positions are randomly selected from the optional position set as candidates, and then the power output of the turbine at the selected candidate position is predicted using the DBO-ELM prediction model. The position with the largest predicted value of the power output is taken as the new position of the previous worst turbine. The process of DBO-ELM-GA is shown in Fig. 2.

3. Case Study

In this section, the simulation environment and the relevant settings of the model are introduced in detail, and the DBO-ELM response surface used to guide GA is exhibited in a visual form.

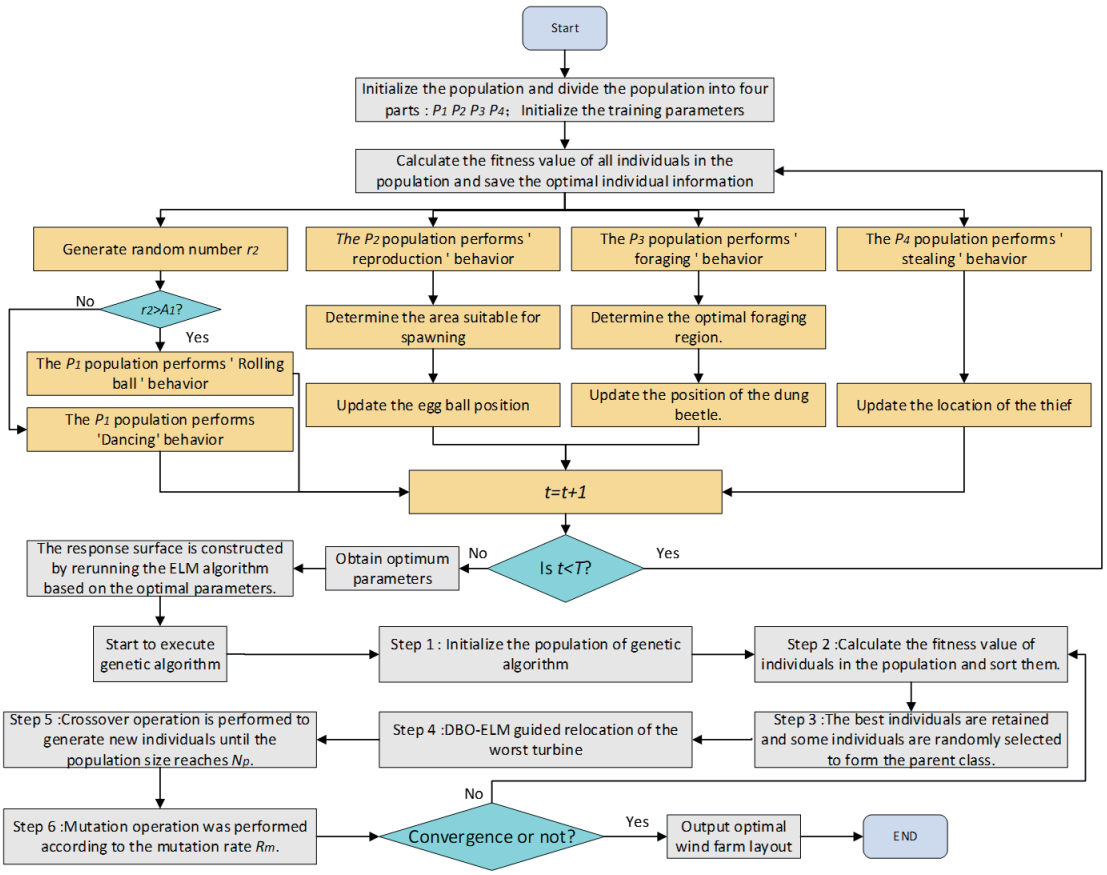

Fig. 2. (Color online) Flow chart of DBO-ELM-GA.

3.1 Simulated environment

In the case study, we build a simulation environment based on Python language to simulate the real wind farm. To verify the versatility of the proposed method, there are three variables in the experiment: the forbidden zone setting of the wind farm, the wind distribution setting, and the number of turbines. For the forbidden zone setting of wind farms, we verify the performance of the algorithm in six wind farms with different forbidden zone settings. The six forbidden zone setting schemes of wind farms are shown in Fig. 3. For the turbine setting scheme, we assume that the specifications and losses of all turbines are the same, but the number of turbines set is different. The performance of the algorithm is tested with the number of turbines set to 15, 20, and 25 under different forbidden zone and wind distribution settings.

3.2 Wind condition settings

To verify the layout optimization ability in wind farms with different wind distribution complexities, we assume that the wind condition distribution data collected by the wind speed and direction sensor are single wind direction (D_1), four wind directions (D_2), and six wind directions (D_3), and the wind speed is set to 13 m/s. Among them, the wind condition distribution D_1 is used to verify the optimization ability in the simplest case of a single wind direction and

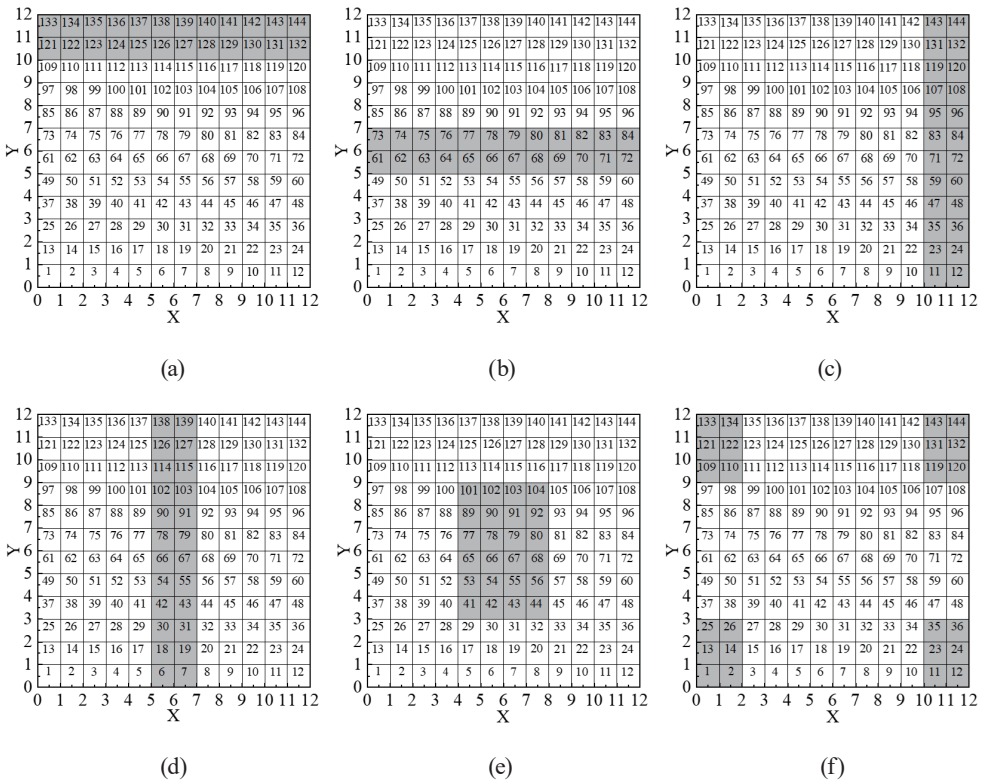

Fig. 3. Schematic diagrams of forbidden zone settings for six different wind farms. Forbidden zone setting scheme (a) L1, (b) L2, (c) L3, (d) L4, (e) L5, and (f) L6.

single wind speed. The wind condition distribution D_2 is set to four wind directions, and the settings of θ are 0, π/2, π, and 3π/2. The probability distribution of each wind direction is shown in Table 1. The wind condition distribution D_1 is set to six wind directions, and θ is set to 0, π/3, 2π/3, π, 4π/3, and 5π/3. The probability distribution of each wind direction is shown in Table 2.

3.3 Wind farm terrain settings

To balance the accuracy and computational cost of the experiment, we set the wind farm as a square and divided it into 144 square units of equal size, with the width of each unit set to 154 m. Since it is impossible to experiment with all the forbidden zone settings, we choose the six representative wind farm forbidden zone settings shown in Fig. 3.

3.4 DBO-ELM response surface

In general, the position with higher expected power is a better position than the randomly selected position. The Monte Carlo simulation can approximate the power distribution of the wind farm. The ELM response surface defined in this study is the wind power distribution of the wind farm, and the role of the DBO algorithm is to improve the performance of the ELM. On the basis of the setting of the case study, all combinations of wind condition distribution, number of turbines, and wind farm exclusion zone settings are generated for corresponding ELM response surfaces, some of which are shown in Figs. 4 and 5.

The generated response surface shows that the expected power generation of turbines in the forbidden zone position is very low. The optimal location of the turbine usually appears in the upstream part of the wind direction. However, when the wind conditions are complex (D_2, D_3), it is impossible to manually select the optimal position so that the assistance of the DBO-ELM response surface is needed.

4. Evaluation of Model Performance

In this section, we use the conversion efficiency η to measure the performance of each layout optimized by the three methods under three wind conditions and different forbidden zone settings. The higher the η, the better the layout. The conversion efficiency formula is

Table 1
Probability distribution of wind direction in wind condition distribution D_2.

Direction	0	π/2	π	3π/2
Population size	25	25	25	25

Table 2
Probability distribution of wind direction in wind condition distribution D_3.

Direction	0	π/3	2π/3	π	4π/3	5π/3
Population size	20	30	20	10	10	10

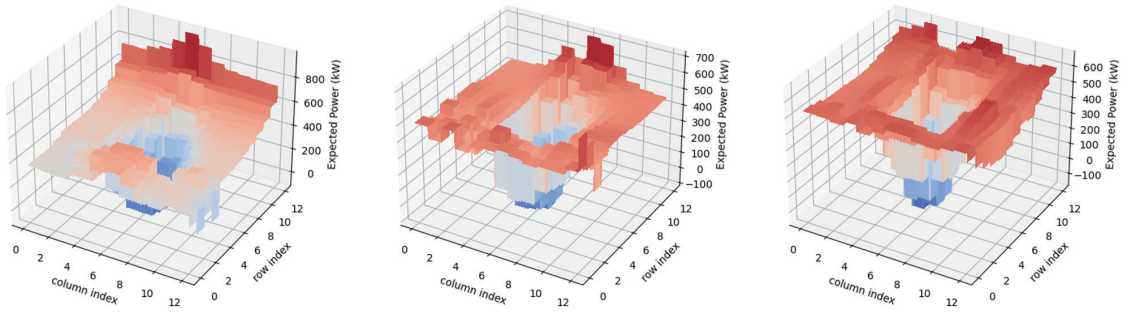

(a) (b) (c)

Fig. 4. (Color online) Response surface of DBO-ELM at L5 with 20 turbines. Wind Profile (a) D_1, (b) D_2, and (c) D_3.

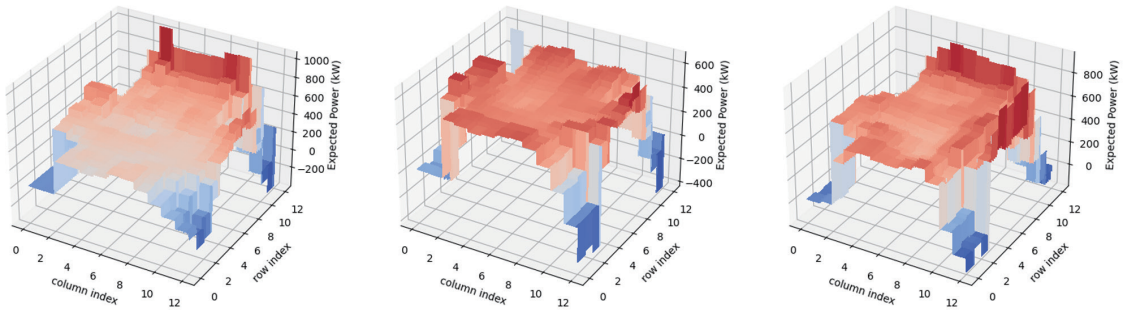

(a) (b) (c)

Fig. 5. (Color online) Response surface of DBO-ELM at L6 with 20 turbines. Wind Profile (a) D_1, (b) D_2, and (c) D_3.

$$\eta = \frac{\vartheta_{tot}\left(N,\phi\right)}{N\sum_{\theta,v} p\left(\theta,v\right)\vartheta_r\left(v\right)}, \tag{12}$$

where $\vartheta_r(v)$ is the output power when the turbine is not affected by the wake effect. $\vartheta_{tot}(N, \phi)$ is set as the total power generation of the wind farm with N turbines in the case of layout ϕ. v and θ are the wind speed and wind direction data obtained by the wind speed and wind direction sensor, respectively. $p(\theta, v)$ is the probability distribution that wind speed v and wind direction θ occur simultaneously. Here, we repeat the test 15 times and compare the average and best results of each method.

4.1 Optimal layout optimization results at D_1

The average and optimal results using three algorithms under 15 tests at D_1 are shown in Tables 3 and 4, respectively, where 'N of T' is the abbreviated form of "the number of turbines". As can be seen, the conversion efficiency decreases with an increase in the number of turbines owing to the interaction of wakes. Also, the conversion efficiency decreases with an increase in

Table 3
Conversion efficiency at D_1 (average).

N of T	15			20			25		
Algorithm	CGA	AGA	DBO-ELM-GA	CGA	AGA	DBO-ELM-GA	CGA	AGA	DBO-ELM-GA
L1	96.5	96.89	96.89	90.72	91.68	91.76	83.28	85.12	85.63
L2	97.54	97.83	97.85	93.39	94.42	94.53	86.68	88.34	88.87
L3	95.51	95.75	95.84	88.6	89.98	90.45	80.32	81.84	82.25
L4	95.32	95.88	95.98	88.51	90.12	90.59	80.73	82.08	82.14
L5	97.57	97.82	97.86	93.47	94.62	94.51	87.4	88.78	89.7
L6	97.28	97.7	97.73	91	92.7	92.4	83.23	84.75	85.7
Mean	96.62	96.98	97.03	90.95	92.25	92.37	83.61	85.15	85.72

Table 4
Conversion efficiency at D_1 (optimal).

N of T	15			20			25		
Algorithm	CGA	AGA	DBO-ELM-GA	CGA	AGA	DBO-ELM-GA	CGA	AGA	DBO-ELM-GA
L1	96.96	96.96	96.96	92.59	92.46	92.66	84.01	86.54	86.54
L2	97.74	97.88	97.89	94.58	94.84	94.92	88.43	89.24	89.66
L3	96.06	96.06	96.06	89.75	91.27	91.32	81.63	82.84	84.24
L4	95.89	96.34	96.34	90.37	91.7	91.96	81.86	83.03	83.2
L5	97.74	97.88	97.88	94.25	95.25	95.35	88.81	90.08	90.9
L6	97.57	97.88	97.88	92.46	93.41	93.94	84.31	86.68	86.68
Mean	96.99	97.17	97.17	92.33	93.16	93.36	84.84	86.40	86.87

the area of the forbidden zone because of the decrease in the number of deployable turbines. It is found that the conversion efficiency is 2% higher than that of L3 on average when the forbidden zone is set to L1 because wind farm L1 is wider than L3 when the wind condition is set to D_1. On the other hand, the conversion efficiency of L2 is 4.23% higher than that of L4, and the highest average conversion efficiency occurs at L5 when the wind condition is set to D_1. To summarize, the conversion efficiency of DBO-ELM-GA is 0.24% higher than that of AGA and 1.31% higher than that of CGA in general.

The optimal layout training process diagram of 25-turbine layout optimization is shown in Fig. 6. As shown in the diagram, in the early stage of training, the training speed of the three algorithms is the fastest, but CGA exhibits difficulty in breaking away from the local optimum. This conclusion is best reflected in the training processes of L1 and L2. For L6, compared with AGA, DBO-ELM-GA introduces the response surface guidance relocation method, so that the algorithm can still explore the optimal layout even if it does not find a better layout in the early training stage.

4.2 Optimal layout optimization results at D_2

Similar to Sect. 5.1, the average and optimal results of the 15 operations of the three algorithms are shown in Tables 5 and 6, respectively. The conversion efficiency decreases with an increase in the number of turbines, and the overall conversion efficiency is lower than D_1.

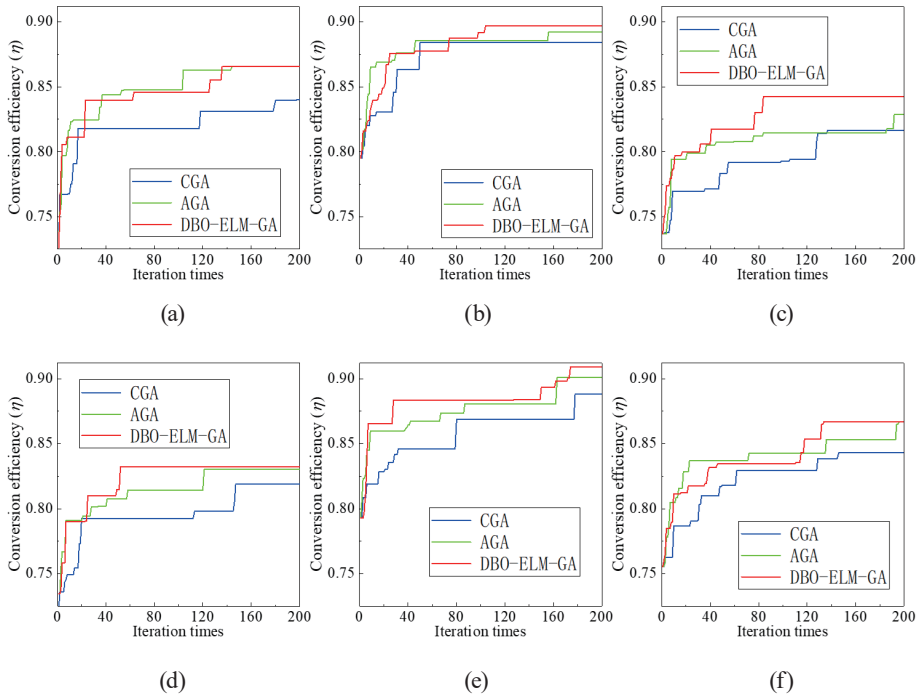

Fig. 6. (Color online) Optimal layout training process with 25 turbines at D_1. Forbidden zone setting scheme (a) L1, (b) L2, (c) L3, (d) L4, (e) L5, and (f) L6.

Table 5
Conversion efficiency at D_2 (average).

N of T	15			20			25		
Algorithm	CGA	AGA	DBO-ELM-GA	CGA	AGA	DBO-ELM-GA	CGA	AGA	DBO-ELM-GA
L1	91.73	93.46	93.79	82.92	85.44	85.84	75.59	77.64	77.9
L2	92.82	94.46	94.74	85.09	87.26	87.71	77.61	80.15	80.34
L3	92	93.72	93.77	83.29	85.54	85.64	75.42	77.8	78.14
L4	92.98	94.58	94.64	84.82	87.28	87.5	77.87	80.15	80.49
L5	93.17	94.73	95.27	85.92	87.99	88.32	89.98	81.71	81.79
L6	93.99	95.54	95.55	85.79	88.34	88.51	78.52	80.69	81.18
Mean	92.78	94.42	94.63	84.64	86.98	87.25	79.17	79.69	79.97

Table 6
Conversion efficiency at D_2 (optimal).

N of T	15			20			25		
Algorithm	CGA	AGA	DBO-ELM-GA	CGA	AGA	DBO-ELM-GA	CGA	AGA	DBO-ELM-GA
L1	92.86	94.44	94.95	84.02	86.42	86.58	76.59	78.19	78.6
L2	93.51	95.27	95.42	86.24	88.09	88.37	79.26	80.72	80.97
L3	93.02	94.18	94.38	84.11	86.15	86.5	76.75	78.52	78.63
L4	93.83	94.87	95.02	85.81	87.79	87.94	78.81	80.63	81.4
L5	94.19	95.05	95.88	86.74	88.41	88.64	80.34	82.12	82.35
L6	95.35	96.23	96.47	87.63	88.85	89.42	81.37	81.25	82.08
Mean	93.79	95.01	95.35	85.76	87.62	87.91	78.85	80.24	80.67

The conversion efficiency difference between L1 and L3 is not significant, with the average conversion efficiency difference being 0.17%. The conversion efficiencies of L2 and L4 are also very close, and the average conversion efficiency is 0.02%, which is different from that when the wind condition distribution is D_1, because the four wind farms L1–L4 have the same width under D_2 distribution. Similarly to D_1, L5 is still the wind farm with the highest average conversion efficiency, indicating that the availability of the central area in the wind farm has little effect on the optimal layout when the wind condition distribution is D_2. However, unlike D_1, L6 is the wind farm with the second highest average conversion efficiency, which indicates that the influence of the availability of the four corners on the turbine layout is much lower than that of D_1 when the wind condition distribution is D_2.

The average optimization result of CGA is the lowest, and that of DBO-ELM-GA is the highest. Note that when the number of turbines to be optimized is 15, 20, and 25, the optimization results of DBO-ELM-GA are 0.21%, 0.27%, and 0.28% higher than those of AGA on average, which indicates that the more turbines to be optimized, the more obvious the advantages of DBO-ELM-GA.

The optimal layout training process diagram for 25-turbine layout optimization is shown in Fig. 7. In the training process of the optimal results, only DBO-ELM-GAs with forbidden zones set to L2 and L4 quickly converge to the optimal layout within 100 rounds, and for other wind farms, convergence to the optimal layout occurs in the second half. This reveals that DBO-ELM-GA can still learn the optimal layout even though the layout of the initial training stage is slightly

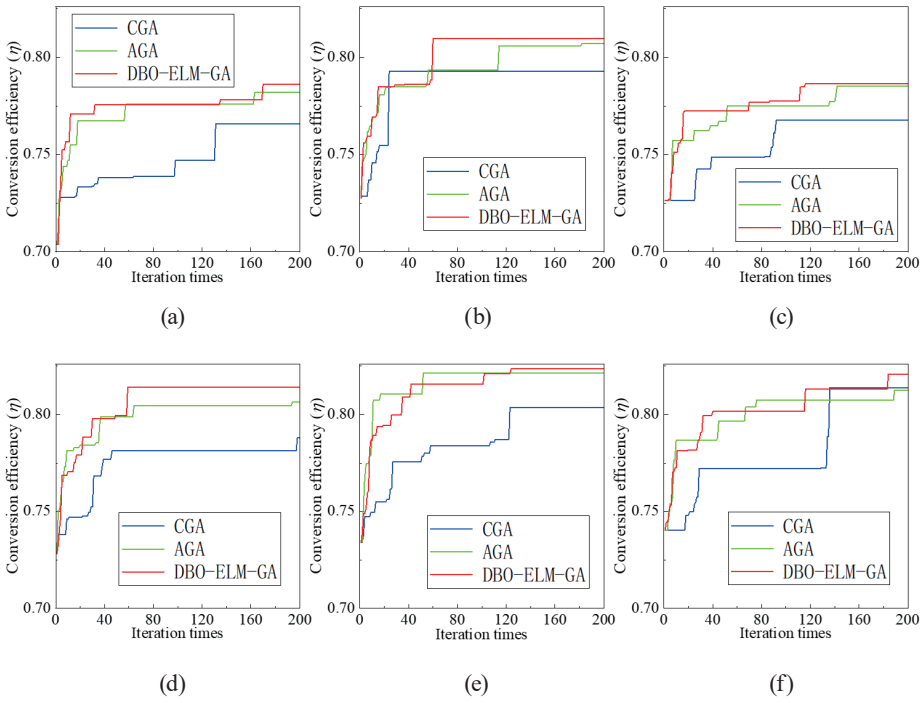

Fig. 7. (Color online) Optimal layout training process with 25 turbines at D_2. Forbidden zone setting scheme (a) L1, (b) L2, (c) L3, (d) L4, (e) L5, and (f) L6.

worse than those of other algorithms, that is, the algorithm has high robustness and does not easily fall into a local optimum.

4.3 Optimal layout optimization results at D_3

The three GAs are tested on wind farms when the wind condition distribution is set to D_3. The average and optimal results of the three algorithms for 15 runs are shown in Tables 7 and 8, respectively. Among the three wind conditions, the overall conversion efficiency under the D_3 setting is the highest. Even if the conversion efficiency decreases with an increase in the number of turbines to be optimized, the proportion of reduction is much smaller than those in the cases of D_1 and D_2 wind conditions. The average conversion efficiency of the three algorithms is the highest when the forbidden zone is set to L2 and L5, which indicates that the influence of the availability of the middle position of the wind farm on the power output is relatively small when the wind condition distribution is D_3. L6 has the lowest conversion efficiency in six wind farms, which indicates that there is a considerable influence on the output power of the optimized wind farm regardless of whether or not the edge position is available.

The comparison of the optimization results of the three algorithms when the wind condition distribution is set to D_3 shows that DBO-ELM-GA has the highest average and optimal conversion efficiency under all forbidden zone settings and turbine number settings. The average

Table 7
Conversion efficiency at D_3 (average).

N of T	15			20			25		
Algorithm	CGA	AGA	DBO-ELM-GA	CGA	AGA	DBO-ELM-GA	CGA	AGA	DBO-ELM-GA
L1	97.3	98.55	98.61	93.42	96.07	96.77	89.52	93.4	94.09
L2	97.86	98.98	99.15	95.18	96.9	97.41	91.59	94.77	95.33
L3	97.17	98.3	98.72	93.49	95.78	96.28	89.81	92.45	93.12
L4	97.14	98.41	98.63	93.76	95.69	96.09	90.3	92.66	93.1
L5	98.06	99	99.11	94.78	97.16	97.6	91.46	94.53	94.94
L6	97.17	98.28	98.56	93.46	95.53	96.07	89.86	92.13	92.15
Mean	97.45	98.59	98.80	94.02	96.19	96.709	90.429	93.329	93.79

Table 8
Conversion efficiency at D_3 (optimal).

N of T	15			20			25		
Algorithm	CGA	AGA	DBO-ELM-GA	CGA	AGA	DBO-ELM-GA	CGA	AGA	DBO-ELM-GA
L1	98.33	98.72	98.88	94.63	96.91	97.4	90.4	94.06	95.75
L2	99	99.28	99.36	96.45	97.48	98.16	92.9	95.36	96.13
L3	97.86	98.75	98.94	94.33	96.71	97.11	91.39	93.02	93.85
L4	98.51	98.87	98.94	95	96.35	96.84	90.82	93.52	93.97
L5	98.73	99.24	99.36	95.8	97.65	98.02	92.61	95.58	96.01
L6	97.92	98.49	98.98	94.31	96.01	96.92	91.34	93.01	93.25
Mean	98.39	98.89	99.08	95.09	96.85	97.41	91.58	94.09	94.83

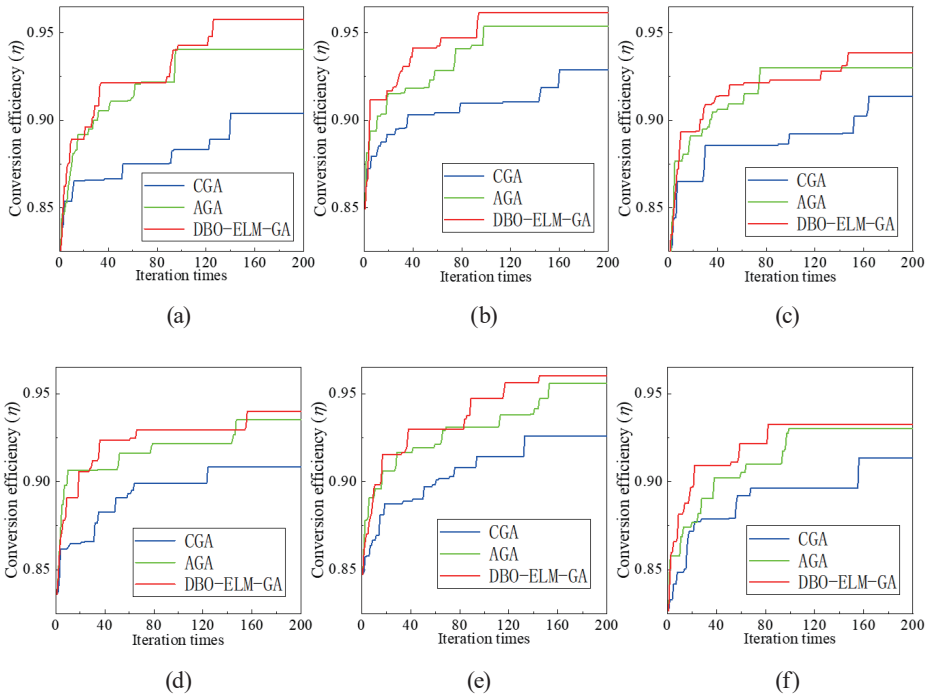

Fig. 8. (Color online) Optimal layout training process with 25 turbines at D_3. Forbidden zone setting scheme (a) L1, (b) L2, (c) L3, (d) L4, (e) L5, and (f) L6.

conversion efficiencies are 0.4% and 2.47% higher than those of AGA and CGA, respectively. Among them, DBO-ELM-GA has the largest average conversion efficiency improvement of 0.53% compared with AGA in L3 wind farms, and the second largest improvement of 0.48% compared with L1. When compared with CGA, the improvement is the largest in L1 at 3.08% and second largest in L3 at 2.55%. The comparison results of the optimal layout conversion efficiency reveal that DBO-ELM-GA shows the most obvious improvements of 0.78% and 2.89% in the conversion efficiency compared with AGA and CGA in the wind farm with the forbidden area set to L1, respectively.

The optimal layout training process diagram for 25-turbine layout optimization is shown in Fig. 8. Under this wind condition distribution, DBO-ELM-GA can obtain a layout with better conversion efficiency than AGA and CGA at the initial stage of training (within 60 rounds). The advantage can be maintained until the end of training, yielding the optimal layout. This result indicates that the response-surface-guided relocation method can enable the algorithm to easily explore a better layout.

5. Conclusions

Our proposed model to minimize the wake effect, based on a combination of the AGA, ELM, and DBO algorithms, showed good performance. The major contributions of this study are summarized as follows.

(1) DBO-ELM-GA can generally increase the conversion efficiency of the wind farm to 1.85% and 0.3% higher than those of CGA and AGA, respectively, on average at D_1, D_2, and D_3.
(2) DBO-ELM-GA has extremely high robustness. It can continue to train a layout with increasing conversion efficiency when the layout at the initial stage of training is suboptimal. More benefits can be achieved especially under complex wind distribution.
(3) The reduction of the wake effect as well as better power generation layout have been achieved for six different wind farms under three different wind condition distributions.
(4) Whether or not the central area is available in the wind farm has little impact on the conversion efficiency.

In future work, further study is suggested to (1) make the simulation environment more realistic by using a more complex combined model, (2) develop better guidance methods to optimize GAs or use other intelligent optimization algorithms to solve wind farm layout problems, and (3) improve the performance of ELM and explore other guidance models.

Acknowledgments

This study was supported by "Chunhui Program" Collaborative Scientific Research Project of the Ministry of Education of the People's Republic of China [Project No. HZKY20220242] and the S&T Program of Hebei [Project Nos. 21567605H and 225676163GH].

References

1 S. H. Yang, K. Yang, X. W. Deng, and J. Yang: Energy Convers. Manage. **285** (2023) 116949. https://doi.org/10.1016/j.enconman.2023.116949
2 Z. C. Liang and H. X. Liu: Energies **16** (2023) 5916. https://doi.org/10.3390/en16165916
3 F. Y. Bai, X. L. Ju, S. Y. Wang, W. Y. Zhou, and F. Liu: Energy Convers. Manage. **252** (2022) 115047. https://doi.org/10.1016/j.enconman.2021.115047
4 S. Lumbreras and A. Ramos: IEEE Trans. Power Syst. **28** (2013) 1434. https://doi.org/10.1109/TPWRS.2012.2204906
5 A. H. Schrotenboer, E. Ursavas, and I. F. A. Vis: Transp. Res. Part C Emerging Technol. **112** (2020) 180. https://doi.org/10.1016/j.trc.2019.12.014
6 Y. Yu, T. F. Zhang, Z. Y. Lei, Y. R. Wang, H. C. Yang, and S. C. Gao: Appl. Soft. Comput. **141** (2023) 110306. https://doi.org/10.1016/j.asoc.2023.110306
7 A. Kusiak and Z. Song: Renewable Energy **35** (2010) 685. https://doi.org/10.1016/j.renene.2009.08.019
8 Y. Eroglu and S. U. Seckiner: Renewable Energy **44** (2012) 53. https://doi.org/10.1016/j.renene.2011.12.013
9 Z. Y. Lei, S. C. Gao, Z. M. Zhang, H. C. Yang, and H. T. Li: IEEE/CAA J. Autom. Sin. **10** (2023) 1168. https://doi.org/10.1109/JAS.2023.123387
10 J. Song, T. Kim, and D. You: Renewable Energy **206** (2023) 738. https://doi.org/10.1016/j.renene.2023.02.058
11 J. Serrano González, Á. L. Trigo García, M. Burgos Payán, J. Riquelme Santos, and Á. G. González Rodríguez: Appl. Energy **200** (2017) 28. https://doi.org/10.1016/j.apenergy.2017.05.071
12 Z. Q. Liu, S. L. Fan, Y. Z. Wang, and J. Peng: Energy Convers. Manage. **245** (2021) 114610. https://doi.org/10.1016/j.enconman.2021.114610
13 G. Mosetti, C. Poloni, and B. Diviacco: J. Wind Eng. Ind. Aerodyn. **51** (1994) 105. https://doi.org/10.1016/0167-6105(94)90080-9
14 A. S. O. Ogunjuyigbe, T. R. Ayodele, and O. D Bangboje: Front. Energy **15** (2021) 240. https://doi.org/10.1007/s11708-018-0514-x
15 Y. H. Ma, K. G. Xie, Y. A. Zhao, H. J. Yang, and D. B. Zhang: CSEE J. Power Energy Syst. **8** (2022) 1623. https://doi.org/10.17775/CSEEJPES.2020.03350
16 L. C. Cao, M. W. Ge, X. X. Gao, B. W. Du, B. L. Li, Z. Huang, and Y. Q. Liu: Appl. Energy **323** (2022) 119599. https://doi.org/10.1016/j.apenergy.2022.119599

17 X. L. Ju, F. Liu, L. Wang, and W. J. Lee: Energy Convers. Manage. **196** (2019) 1267. https://doi.org/10.1016/j.enconman.2019.06.082
18 T. A. Qureshi and V. Warudkar: Environ. Sci. Pollut. Res. **30** (2023) 77436. https://doi.org/10.1007/s11356-023-27849-7
19 F. Liu and Z. Wang: arXiv (2014). https://doi.org/10.48550/arXiv.1403.7178
20 Y. Niu, P. P. Lathi, and R. Nagamune: IEEE: Proc. 2023 American Control Conference. (IEEE, 2023) 2542–2547.
21 N. Jensen: Risø-M 2411 (1983).
22 J. Xue and B. Shen: J. Supercomput. **79** (2023) 7305. https://doi.org/10.1007/s11227-022-04959-6
23 G.-B. Huang, Q.-Y. Zhu, and C.-K. Siew: Neurocomputing **70** (2006) 489. https://doi.org/10.1016/j.neucom.2005.12.126
24 K. Binder, D. Heermann, L. Roelofs, A. J. Mallinckrodt, and S. McKay: Computer in Physics **7** (1993) 156. https://doi.org/10.1063/1.4823159